

SUPERSTRONG LIGHT FIELDS

PACS numbers: 79.20.Eb; 81.07.-b; 42.65.Re
DOI: 10.1070/QE2015v045n06ABEH015771

Formation of nanostructures under femtosecond laser ablation of metals

S.I. Ashitkov, S.A. Romashevskii, P.S. Komarov, A.A. Burmistrov, V.V. Zhakhovskii, N.A. Inogamov, M.B. Agranat

Abstract. **We present the results of studying the morphology of the modified surface of aluminium, nickel and tantalum after ablation of the surface layer by a femtosecond laser pulse. The sizes of characteristic elements of a cellular nanostructure are found to correlate with thermo-physical properties of the material and the intensity of laser radiation.**

Keywords: *femtosecond laser pulse, ablation, nanostructures.*

1. Introduction

In recent years, femtosecond lasers have been increasingly used for a wide range of problems associated with precision machining, as well as for creation of functional materials with specific optical and thermal properties [1–7]. In contrast to the process of evaporation of a material exposed to millisecond and nanosecond laser pulses, the main mechanism responsible for removing a material in the case of femtosecond pulses is thermomechanical ablation, caused by the action of high tensile stresses on the surface layer. Currently, the processes of nonequilibrium heating of electrons and the lattice, material melting and expansion under the action of femtosecond pulses is studied in detail [8–12]. However, the final stage of the ablation process associated with the formation of surface nanostructures is poorly investigated. In particular, the theoretical analysis of this phenomenon requires large amounts of computing resources in the molecular dynamics (MD) simulations. The MD methods, because of their atomistic nature where an interatomic interaction potential plays the fundamental role, reproduce in the most realistic way strongly nonequilibrium processes and metastable states of matter, arising in a thin surface layer after irradiation. Hydrodynamic modelling of such processes as ultrafast melting, melt tension and loss of continuity with the formation of cavitation bubbles is rather cumbersome, while they are relatively simply implemented in MD calculations. This paper deals with the experimental study of the properties of the formation of surface nanostructures under thermomechanical ablation of metals, as well as the influence of parameters of femtosecond pulses and material properties on the morphology of the surface nanorelief formed.

The impact of an ultrashort laser pulse on a metal sample initiates a series of physical processes, which finally can lead to the formation of a target surface with complex morphology [13–15]. Immediately after irradiation, in a thin surface layer there appears a two-temperature state when the temperatures of the electron and ion subsystems are different. During electron–ion thermalisation and diffusion of heat inside a material, there occurs bulk melting of a superheated layer and temperature and pressure profiles are formed. Then, compression and tension waves begin to spread deep into a sample, creating high tensile stresses that reach a maximum in the subsurface layer at a depth of several tens of nanometres, which initiates the nucleation of vapour bubbles in the melt. As a result of their growth and aggregation during cavitation, a foam material with complex cellular structure is formed. During the time from a few tens to hundreds of picoseconds, a thin liquid ablation layer separated from the basic material of the target by a layer of foamed melt is formed on the target surface. The evolution of the foam and its decomposition are determined by the mass and the temperature of the substance involved in the cavitation processes and is dependent on the absorbed laser energy and thermophysical and mechanical properties of the material. The subsequent expansion of the foam is accompanied by thinning of the walls of the cells and their rupture with the formation of filaments and drops. At the same time, heat conduction processes lead to a cooling of the liquid phase and the final formation of the surface nanorelief.

2. Experiment

In this paper, nanostructures on the surface of metal film samples were formed with the help of radiation from a Ti : sapphire laser with a pulse duration of 40 fs at a wavelength of 800 nm. The samples were ~1-μm-thick aluminium, nickel and tantalum films deposited by magnetron sputtering on polished glass substrates. A beam of p-polarised laser radiation was focused on the sample surface by a lens with a focal length $f = 30$ cm at an angle of 45°. The spatial distribution in the focal spot corresponded to Gaussian with a radius $r_0 = 30$ μm at the e^{-1} level. The experiments were conducted in the air at different laser pulse energy densities F in the regime of a single exposure. The morphology of surface nanostructures in the irradiated regions was studied using a Tescan Mira 3 scanning electron microscope (SEM).

S.I. Ashitkov, S.A. Romashevskii, P.S. Komarov, A.A. Burmistrov, M.B. Agranat Joint Institute for High Temperatures, Russian Academy of Sciences, ul. Izhorskaya 13, Bld. 2, 125412 Moscow, Russia; e-mail: ashitkov11@yandex.ru;
V.V. Zhakhovskii N.L. Dukhov All-Russian Research Institute of Automatics, Sushchevskaya ul. 22, 127055 Moscow, Russia; e-mail: 6asi1z@gmail.com;
N.A. Inogamov L.D. Landau Institute for Theoretical Physics, Russian Academy of Sciences, prosp. Akad. Semenova 1-A, 142432 Chernogolovka, Moscow region, Russia; e-mail: nailinogamov@gmail.com

Received 29 January 2015; revision received 10 February 2015
Kvantovaya Elektronika **45** (6) 547–550 (2015)
Translated by I.A. Ulitkin

Figure 1 shows SEM images of a modified surface of an aluminium target in the central part of the ablation crater after exposure to a femtosecond pulse with a varying energy density F. It can be seen that the modified surface of the bottom of the ablation crater has a rather complex morphology. The main basic elements are cellular structures in the form of polyhedrons, which represent the remains of broken and subsequently frozen membranes of nanofoam cells. Another characteristic element is spherical formations, formed from the melt after the rupture of membranes under the action of surface tension forces. Furthermore, at a large excess of F over the ablation threshold F_a (Fig. 1b), the proportion of ablative 'debris' in the form of nanospheres measuring from a few to tens of nanometres, deposited on the surface, increases. Thus there is a clear trend of increasing characteristic sizes of cellular and spherical nanostructures with increasing laser radiation intensity. The size of individual cells on the surface of aluminium increases from tens or hundreds of nanometres at a density F near F_a to micrometres at $F/F_a \geqslant 5$ (Fig. 2).

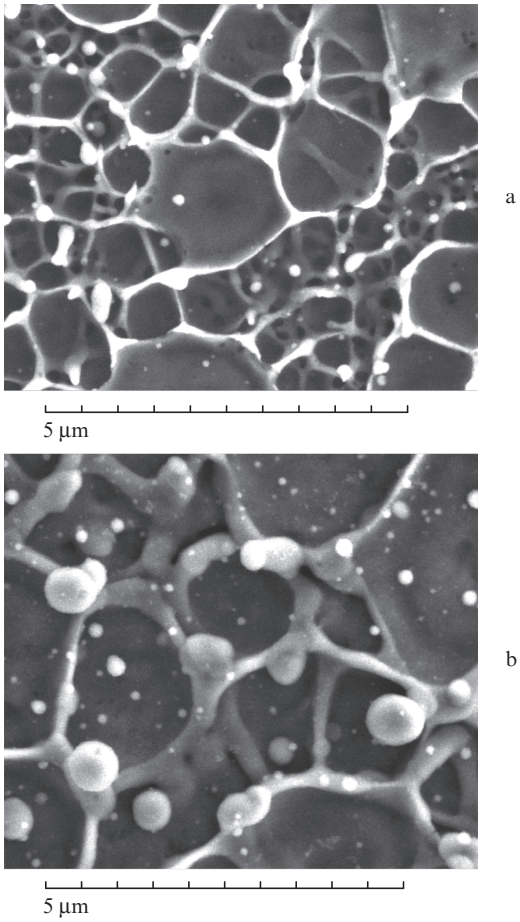

Figure 1. SEM images of the fragments of the central part of ablation craters formed on the surface of an aluminium sample after exposure to a laser pulse with a varying energy density at F/F_a = (a) 2 and (b) 3.6.

Figure 3 shows SEM images of the central part of a modified surface of nickel and tantalum samples after exposure to a femtosecond pulse with an energy density $F/F_a = 2$. Note that the images in Figs 1 and 3 were obtained at different magnifications.

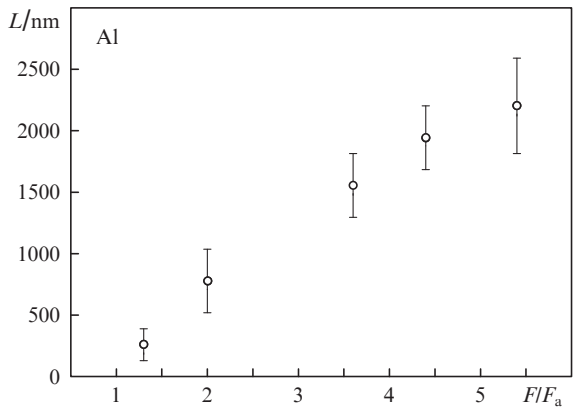

Figure 2. Characteristic size L of cellular structures of the modified aluminium surface as a function of the excess of the femtosecond pulse energy density over the ablation threshold after single pulse irradiation of the target.

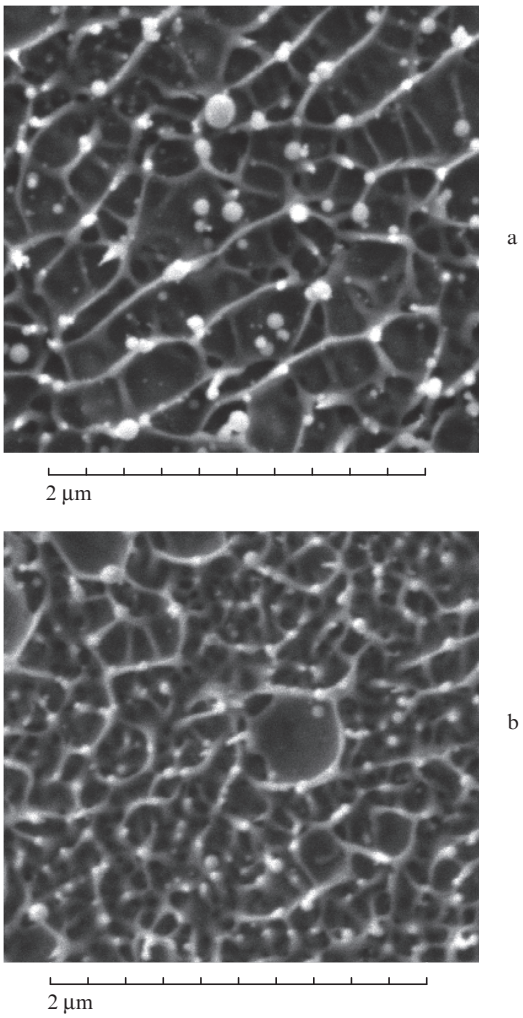

Figure 3. SEM images of the central part of craters on (a) nickel and (b) tantalum at $F/F_a = 2$.

Noteworthy is approximately the same morphology of the modified surface of the materials in question; however, the characteristic sizes of cellular structures differ markedly. With the same parameter $F/F_a = 2$, the largest cell size

(0.5–1 μm) was observed for the aluminium sample, and the smallest (100–200 nm) – for tantalum.

3. Results and discussion

The MD method for calculating the ablation process of a metal, caused by rapid heating of a surface layer, is well known and has been previously described in the literature (see, for example, [13, 16]). Figure 4 shows the results of MD calculations of the morphology of the surface relief resulting from femtosecond ablation of an aluminium crystal. In the calculations we used a many-body EAM potential, developed in [16] for the simulation of aluminium at high pressures and strains up to the values corresponding to the theoretical tensile strength. The simulation was performed at an initial sample measuring $L_x \times L_y \times L_z = 500 \times 240 \times 24$ nm for 1.72×10^8 atoms in a simulation box with periodic boundary conditions along the y and z axes. The calculations were made for a ratio of the pulse energy density to the pulse ablation threshold $F/F_a \approx 1.8$. According to the calculations, in this case the foam layer between the expanding liquid ablation layer and the freezing bottom of the future crater begins to disintegrate in about 2 ns after irradiation. As a result, nanostructures in the form of frozen cells of the foam and filaments with droplets at their ends are formed at the bottom of the crater. Figure 4 shows the final stage of the MD calculation in 2.5 ns after laser exposure. On the left is a map of the potential energy of atoms, and on the right is a map of a centrally symmetric atomic order parameter. The structure of the frozen filaments and the surface layer of a few tens of nanometres in thickness is significantly modified and composed of nanosized crystal grains. The interior of the crystal is single-crystalline. Due to poor heat dissipation the droplet at the end of the filament remains liquid by that time and is crystallised later.

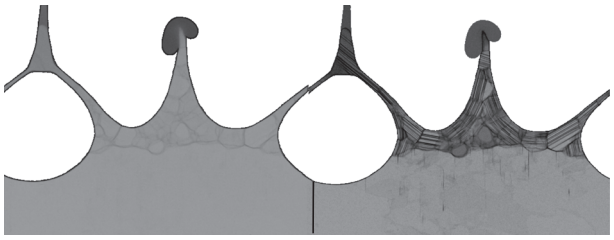

Figure 4. Morphology of the solidifying surface of the aluminium target in 2.5 ns after irradiation during the MD simulation of ablation at $F/F_a = 1.8$; the horizontal size of the calculation domain is 240 nm, and the bubble diameter is about 100 nm.

At an energy density of the femtosecond pulse near the ablation threshold, $F \approx F_a$, the characteristic time of the evolution of bubbles is determined by the stopping time of the motion of a liquid shell separated from the cavitation-unaffected material by a layer of bubbles, i.e., the transition time of the initial kinetic energy of the ablative shell into the potential energy of the surface tension of bubbles of the cavitation layer. The maximum bubble size l in a direction perpendicular to the surface will be expressed as:

$$l \sim \frac{d_T(F - F_c)}{\sigma}, \tag{1}$$

and the time of evolution of bubbles

$$\tau \sim \frac{\rho^{1/2} d_T^{3/2} \sqrt{F - F_c}}{\sigma}, \tag{2}$$

where σ is the surface tension of the melt, and d_T is the depth of warming of the sample at the beginning of cavitation. Cavitation in the melt occurs when the energy density exceeds the cavitation threshold F_c, which is greater than the value F_m, necessary for melting, but smaller than the ablation threshold: $F_a > F_c > F_m$. Given that the surface temperature T_s is approximately proportional to the absorbed energy density, it is possible to conclude that the characteristic time of the collapse of the foam cells slowly increases as $\sqrt{T_s - T_c}$ (T_c is the temperature of cavitation), while the freezing time is growing rapidly as $(T_s - T_m)^2$, where T_m is the melting point. As a consequence, in the annular region of the focal spot on the target, where $F_c < F < F_a$, the surface with subsurface bubbles, frozen at the time when their volume is maximal, may experience a maximum rise. In this case, a rim with a maximum located at a certain distance from the crater walls is formed around the crater, as is the case in aluminium [14]. However, if the freezing occurs across the entire surface of the bubbles in the expansion phase, the maximum of the surface rise is always on the walls of the crater at $F = F_a$. It is also possible that in some materials the bubbles will always collapse faster than the freezing at $F < F_a$. In this case, the formation of neither subsurface frozen bubbles nor rims around the crater is possible.

It should be noted that cellular structures for aluminium are considerably greater than for nickel and tantalum (see Fig. 1a and Fig. 3). This difference at a slight excess of F over the ablation threshold, according to relation (1), can be explained by differences in the surface tension coefficient σ of the melt and the thermal conductivity λ (the latter coefficient determines the depth of warming d_T). The corresponding values of these parameters for the materials in question are as follows [17]: for aluminium $\sigma \approx 0.92$ N m^{-1} (660 °C), $\lambda \approx 230$ W m^{-1} K^{-1}; for nickel $\sigma \approx 1.74$ N m^{-1} (1550 °C), $\lambda \approx 70$ W m^{-1} K^{-1}; and for tantalum $\sigma \approx 2.25$ N m^{-1} (2990 °C), $\lambda \approx 60$ W m^{-1} K^{-1}. Here, the values of σ are taken in the vicinity of the melting point.

At large excesses of the ablation threshold, $F \gg F_a$, the analysis is difficult due to the fact that with increasing F a complex multi-tier foam is formed, consisting of several layers of bubbles. Its disintegration according to the MD calculations for aluminium begins at those places where the walls are thinned down to a few nanometres upon reaching a certain critical bubble size equal to $\sim 10 d_T$. This correlates well with the experimentally determined characteristic sizes of cellular nanostructures in Figs 1 and 2. In this case, the dimensional evaluation of the time of the start of the foam collapse does not contain the coefficient σ:

$$\tau \sim \rho^{1/2} d_T^{3/2} (F - F_c)^{1/2}, \tag{3}$$

because the surface tension forces cannot seriously slow down the stretching of the foam. In the case of a multi-tier foam formed at high absorbed fluences, the primary rapture is likely to occur on the upper floors, where the walls of the cells are hotter and thus less strong. In this case, the central part of the crater has a more complex surface morphology, characterised by large cavities and filaments, as well as by a significant amount of 'debris', dropped out of the collapsed foam from the upper tiers (see Fig. 1b). Thus, the above analysis shows that the final morphology of the modified surface is determined by the ratio of the characteristic times of the cool-

ing of the surface layer and the evolution of the foam layer, which in turn depend on the thermomechanical properties of the material and the absorbed femtosecond pulse energy density.

4. Conclusions

The results of SEM studies of the bottom surface of ablation craters formed after irradiation of metal samples by a single femtosecond pulse have shown that its morphology is characterised by the presence of chaotic cellular nanostructures, the characteristic size of which depends on the material properties and the energy density of laser pulses. According to the molecular dynamics calculations, these structures are formed from the molten foam after its solidification.

Acknowledgements. The work was supported by the ROSATOM State Nuclear Energy Corporation (State Contract No. N.4kh.44.90.13.1111), the Presidium of the Russian Academy of Sciences (Extreme Light Fields and Their Applications Programme) and the Russian Foundation for Basic Research (Grant No. 13-08-01095).

References

1. Furusawa K., Takahashi K., Kumagai H., et al. *Appl. Phys. A*, **69**, S359 (1999).
2. Sanner N., Huot N., Audouard E., et al. *Appl. Phys. B*, **80**, 27 (2005).
3. Eaton S.M., Zhang H.B., Herman P.R. *Opt. Express*, **13**, 4708 (2005).
4. Vorobyev A.Y., Guo C. *Appl. Phys. Lett.*, **86**, 011916 (2005).
5. Wang J., Guo C. *Appl. Phys. Lett.*, **87**, 251914 (2005).
6. Golosov E.V., Emel'yanov V.I., Ionin A.A., et al. *Pis'ma Zh. Eksp. Teor. Fiz.*, **90**, 116 (2009).
7. Wu C., Crouch C.H., Zhao L., et al. *Appl. Phys. Lett.*, **78**, 1850 (2001).
8. Sokolowski-Tinten K., Bialkowski J., Cavalleri A., et al. *Phys. Rew. Lett.*, **81**, 224 (1998).
9. Ivanov D.S., Zhigilei L.V. *Phys. Rev. B*, **68**, 064114 (2003).
10. Bulgakova N.M., Stoian R., Rosenfeld A., et al. *Phys. Rev. B*, **69**, 054102 (2004).
11. Agranat M.B., Anisimov S.I., Ashitkov S.I., et al. *Appl. Surf. Sci.*, **253**, 6276 (2007).
12. Povarnitsyn M.E., Itina T.E., Sentis M., et al. *Phys. Rev. B*, **75**, 235414 (2007).
13. Demaske B.J., Zhakhovsky V.V., Inogamov N.A., et al. *Phys. Rev. B*, **82**, 064113 (2010).
14. Ashitkov S.I., Inogamov N.A., Zhakhovsky V.V., et al. *Pis'ma Zh. Eksp. Teor. Fiz.*, **95**, 192 (2012).
15. Inogamov N.A., Petrov Yu.V., Khokhlov V.A., et al. *J. Opt. Technol.*, **81**, 233 (2014).
16. Zhakhovskii V.V., Inogamov N.A., Petrov Yu.V., et al. *Appl. Surf. Sci.*, **255**, 9592 (2009).
17. Grigoriev I.S., Meilikhov E.Z. (Eds.) *Handbook of Physical Quantities* (Boca Raton: CRC Press, 1997; Moscow: Energoatomizdat, 1991).